

Spatial and Temporal Averages in Chaotic Patterns

Li Ning, Yuchou Hu,* Robert E. Ecke, and Guenter Ahlers

Physics Division and Center for Nonlinear Studies, Los Alamos National Laboratory, Los Alamos, New Mexico 87545

(Received 21 June 1993)

We show that spatiotemporally complex patterns in the presence of a symmetry imposed by the container geometry can have ordered spatial and temporal averages. The system studied was the Küppers-Lortz unstable state in rotating thermal convection. As the control parameter ΔT was increased above onset, fluctuations about the ordered averaged state increased and the correlation of individual patterns with the averaged state decreased. The pattern fluctuations about the averaged state were highly correlated with the instantaneous heat transport fluctuations.

PACS numbers: 47.54.+r, 47.52.+j, 47.27.Te

There has been great interest in the properties of systems that display spatiotemporal chaos, with significant fluctuations in both space and time [1]. An important problem in the study of these complex patterns is finding suitable methods for their analysis. So far relatively standard statistical methods have been used primarily [2-4]. Recently, an experiment on Faraday waves revealed ordered patterns in the long-time averages of individually chaotic patterns as well as some of their properties [5]. Here we explore ways in which such averages are useful in the study of the spatiotemporal dynamics.

Using the Küppers-Lortz (KL) instability [6] in rotating Rayleigh-Bénard convection which produces chaotic pattern dynamics at the onset of convection for sufficiently large rotation rates, we investigated the properties of both spatial and temporal averages. As was done for the Faraday wave case [5], we show that ordered time-averaged patterns with the same symmetry as the sidewalls of the container exist for cells of various shapes and sizes. For very large containers, we find that the ordered averaged structure exists only near the sidewall. We further demonstrate that for patterns with ordered time averages, the *spatial* average of an *instantaneous* pattern along a symmetry direction was essentially the same as this spatial average performed on the time-averaged pattern. This discovery allowed us to investigate the temporal evolution of the spatial average and led to a description of the spatiotemporal behavior of the chaotic patterns.

We also studied the dependence on ΔT of correlations between instantaneous patterns and the ordered time averages. This correlation decreased smoothly as the fluctuation amplitude increased with increasing ΔT until the time averages became featureless. Finally, we show that the fluctuations about the ordered time averages are strongly correlated with variations in the global heat transport.

Our experiments describe the dynamics of patterns in rotating Rayleigh-Bénard convection in a parameter region where the Küppers-Lortz instability produces chaotic dynamics at the onset of convection. The control parameters of the experiment are the top-bottom temperature difference ΔT and the dimensionless rotation rate

$\Omega = \Omega_D d^2/\nu$, where ν is the kinematic viscosity of the working fluid, Ω_D is the angular frequency of the rotating cell, and d is the depth of the fluid layer. We used two fluids, water near 24°C and carbon dioxide at about 20 atm, having quite different fluid properties; the Prandtl number $\sigma = \nu/\kappa$, where κ is the thermal diffusivity, is about 6.4 for water and 0.9 for carbon dioxide. A reduced bifurcation parameter is defined as $\epsilon = [\Delta T - \Delta T_c(\Omega)]/\Delta T_c(\Omega)$, where $\Delta T_c(\Omega)$ is the critical temperature difference for the onset of convection in the interior of the container, i.e., for "bulk convection," at a particular Ω . Over some ranges of rotation rates, this onset can be preceded by a wall convection state consisting of a propagating wave localized radially near the sidewall [7]. The geometry of the convection container is characterized by the aspect ratio $\Gamma = r/d$, where r is the radius of the cylindrical container or, in the general case of a symmetrical polygon, the perpendicular distance from the sidewall to the center. The convection patterns are visualized using digitally enhanced shadowgraph imaging. Details of the setups for the water and carbon dioxide experiments are presented elsewhere [8,9].

The convection containers we used in this series of experiments will be labeled CW (cylindrical, water), CC (cylindrical, CO₂), and HC (hexagonal, CO₂). The critical rotation rate for the KL instability in water (CO₂) is about 23 (13). Container CW ($\Gamma=2.5$) had a sidewall made of 0.31 cm thick and 2 cm high plexiglass which had a lower thermal conductivity than that of the working fluid, water. Containers CC ($\Gamma=4.5$) and HC ($\Gamma=4.4$) were used with pressurized carbon dioxide. Placed inside the active area of a larger convection cell, their sidewalls were made of 0.42 cm high, 0.01 cm thick paper with a higher thermal conductivity than that of the gas. For the range of rotation rates used in the experiments, the instantaneous convection pattern in these relatively small Γ systems consisted of the KL unstable bulk convection rolls coexisting with the sidewall traveling state which was confined near the rigid walls [7]. Another container CC ($\Gamma=41$) which had sidewalls made of paper with a fin extending some distance into the fluid at half height [9] was also used. At the low rotation rates studied for this large container, only bulk convection was

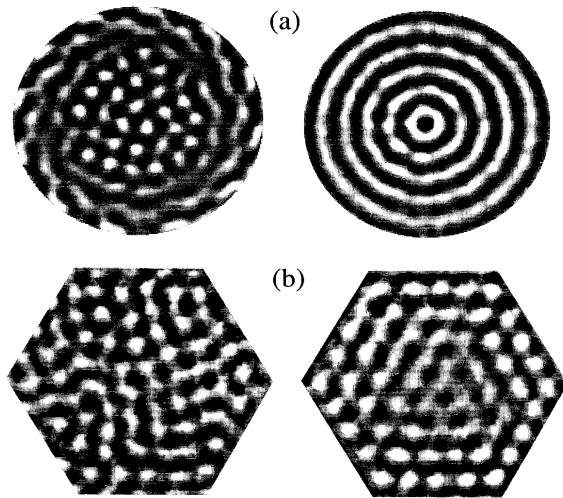


FIG. 1. The instantaneous (left) and time-averaged (right) patterns in rotating Rayleigh-Bénard convection in (a) the cylindrical container CW at $\Omega=1090$ and $\epsilon=0.053$ with water; (b) the hexagonal container HC at $\Omega=150$ and $\epsilon=0.08$ with carbon dioxide.

present.

Ordered time-averaged patterns were found to exist in a range above the onset of convection for all the samples studied, and they all displayed the symmetries of the containers. Two examples are given in Fig. 1. Figure 1(a) shows at left an instantaneous pattern at $\Omega=1090$ and $\epsilon=0.053$ in the cylindrical container CW. The separation between the wall and bulk convection is quite clear. At right the figure shows that the average of 900 patterns taken 120 s apart is a concentric ring pattern. During this period, the rolls and cells of the bulk convection reoriented over 20 times due to the KL instability. The forcing from the boundary produced a phase rigidity of the patterns that manifested itself in the temporal averages. A high degree of phase rigidity of averaged patterns was also observed in Ref. [5]. Figure 1(b) shows instantaneous and averaged patterns over several hundred KL transitions at $\Omega=150$ and $\epsilon=0.08$ in the hexagonal container HC. The averaged pattern shows clearly the hexagonal symmetry of the boundary.

An experiment in a larger container CC ($\Gamma=41$), such as the example in Fig. 2, showed that such averages did not relate trivially to the instantaneous patterns. Here the no-slip boundary conditions tended to force the convection rolls to end perpendicular to the sidewall, yet the time average revealed ring structures parallel to the sidewalls, with an amplitude that decayed in the direction away from the boundary. This result suggests that the ordered averaged patterns which we have observed are unrelated to any symmetries of the underlying chaotic attractor [10]. Previous studies have shown that owing to the mismatch between the thermal properties of the working fluid and the sidewalls, a small horizontal tem-

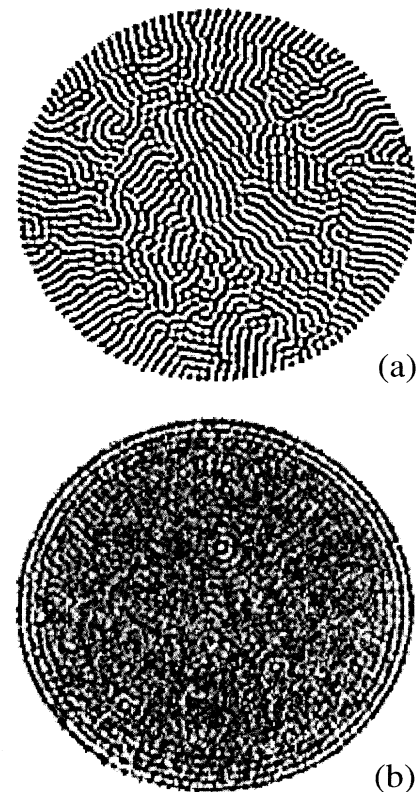


FIG. 2. The instantaneous (top) and time-averaged (bottom) patterns in rotating Rayleigh-Bénard convection in the cylindrical container CC ($\Gamma=41$) at $\Omega=16$ and $\epsilon=0.10$ with CO_2 . The time average is obtained from 720 images covering 6 h.

perature gradient existed from the wall into the bulk of the fluid and caused a weak large-scale circulating flow along that gradient [11]. This in turn caused the convection rolls to orient preferentially parallel to the wall. The above results led us to believe that the ordered time-averaged patterns resulted from such boundary effects, even in the chaotic regime. Since thermal forcing, or boundary effects in general, are extremely hard to eliminate, this study shows that care must be taken to separate bulk pattern dynamics from boundary effects even when the latter are not obvious in the instantaneous patterns.

To study the time-averaged ring pattern for container CW ($\Gamma=2.5$), we averaged the intensity azimuthally and plotted the result in Fig. 3(a). The periodicity was close to the critical wavelength of bulk convection. Also plotted in Fig. 3(a) is the same average for the instantaneous pattern in Fig. 1(a). The two curves are almost identical, demonstrating that the phase rigidity imposed by the sidewall forcing was strong enough to retain the container symmetry in the convection pattern at any instant for this ϵ . The apparently random pattern of the bulk convection was the result of random deviations, both in space and time, from that underlying regular average structure. Similar analysis was performed on the patterns in the

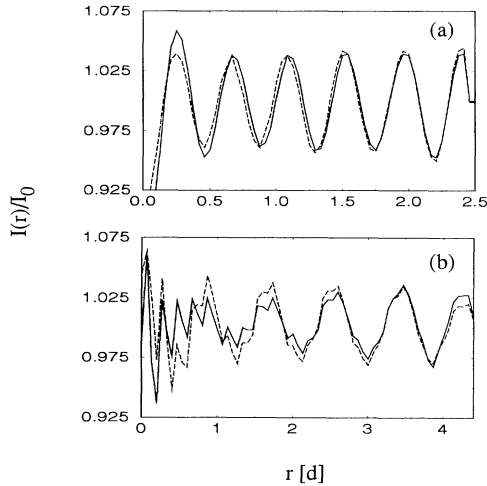


FIG. 3. Spatially averaged intensities for the instantaneous (dashed line) and time-averaged (solid line) convection patterns at (a) $\Omega = 1090$, $\epsilon = 0.053$ in the cylindrical container CW and (b) $\Omega = 150$, $\epsilon = 0.08$ in the hexagonal container HC.

hexagonal container. The spatial averages were carried out along lines parallel to the hexagonal sidewall. The results are shown in Fig. 3(b). The irregularity near the center for patterns in container HC is caused by the imperfect nature of the hexagonal pattern, by the weaker effects of sidewall forcing at the center, and by there being few points available for averaging.

To examine the dynamics of such spatial averages, space-time plots of the azimuthal averages of the instantaneous patterns were generated. Some examples obtained in the cylindrical container CC ($\Gamma = 4.5$) are shown in Fig. 4. Near onset the averaged pattern had 5.5 periods and a corresponding wavelength that was close to the critical wavelength. As ϵ increased, the preferred wavelength of the convection pattern became larger. The number of periods in the averaged pattern started to fluctuate between 5.5 and 5, with the 5.5-period state being the predominant one. Gluckman *et al.* [5] also observed discrete steps in the wave numbers of their patterns as ϵ varied, but do not report fluctuations at constant ϵ . The typical fluctuation frequency of the averaged state increased with increasing ϵ , resulting in weaker patterns in the time average away from the sidewalls. At $\epsilon \approx 0.15$, except for 1 or 2 periods near the boundary, there was no dominant spatial structure left in the spatially averaged state, and there were only 1 or 2 rings near the wall that remained in the time-averaged pattern. To supplement these results, the pattern dynamics in the hexagonal container HC were also explored. We obtained similar results, some of which will be discussed in more detail later. There was no evidence that chaotic patterns could have a regular time-averaged pattern without the influence of boundaries. The above results indicate, however, that it is possible to reduce the spatial dimensionality of spatiotemporal chaotic patterns using symmetries found in

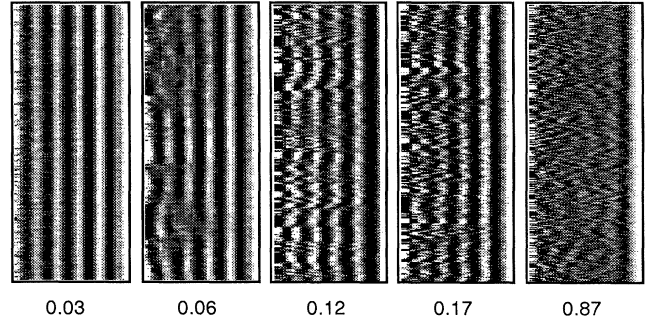


FIG. 4. Space-time plots of the azimuthally averaged intensities of the instantaneous patterns at a few labeled ϵ in the cylindrical container CC ($\Gamma = 4.5$). In each plot, the center of the container is at the left edge and the wall is at the right edge, and time goes up. The time span is 3000 s. All the images are digitally enhanced.

the system geometry.

Using the underlying structural regularity of the patterns as a base, we studied the fluctuations of the patterns and their relationship to the fluctuations of a global property, the instantaneous heat transport. The pixel values of the instantaneous and averaged patterns were assigned the value 0 (1) when they were originally less than (greater than) the mean of the pixel values for that image. At each pair of corresponding pixels of the instantaneous and averaged patterns, 1 and 1 or 0 and 0 were counted as 1, whereas 1 and 0 or 0 and 1 gave -1 . The spatial average $C(t)$ of this resultant pattern represented a measure of the correlation of the instantaneous pattern with its averaged regular pattern: The larger the number was, the less the pattern deviated from the averaged structure. Figure 5 shows the time average \bar{C} for patterns in container CC ($\Gamma = 4.5$). Also shown are the standard deviations δC of $C(t)$, which represent the amplitudes of the fluctuations. The corresponding results for the hexag-

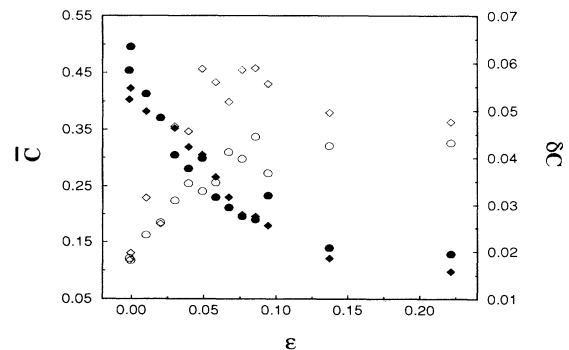


FIG. 5. The mean (\bar{C} , solid symbols) and the standard deviation (δC , open symbols) of the correlations of the instantaneous patterns and the averaged regular pattern in the cylindrical container CC (circles, $\Gamma = 4.5$) and the hexagonal container HC (diamonds, $\Gamma = 4.4$).

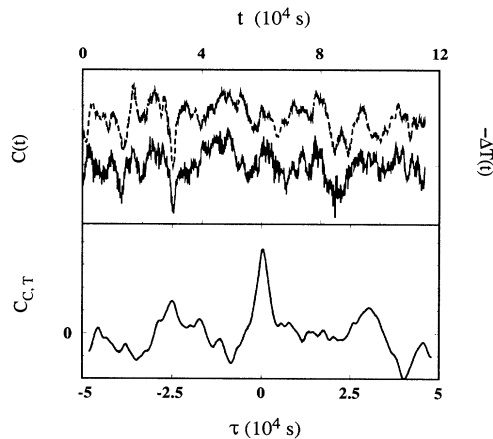


FIG. 6. Top graph: the correlation between instantaneous and averaged patterns (solid line), and the temperature difference across the fluid layer (dashed line, maximum to minimum represents roughly 2 mK), in the cylindrical container CW. Bottom graph: the cross correlation between the two curves in the top figure.

onal container HC are also shown in the figure. Clearly, the mean correlation \bar{C} decreases and the fluctuations δC increase with increasing ϵ . At $\epsilon \approx 0.15$, the mean correlations for both containers reached a base line value, estimated to be 0.1, and the standard deviations saturated. At this point the dominant symmetry-based spatial averages of the patterns disappeared.

Next we studied the cross correlation between fluctuations of the patterns and the instantaneous heat transport of the system. We used the previously obtained $C(t)$, and $\Delta T(t)$, for the container CW experiment. The top graph in Fig. 6 shows the fluctuations around the mean of such time series for $\Omega = 1090$, $\epsilon = 0.053$. The curves look qualitatively similar to the result for $C(t)$ reported at one value of ϵ in Ref. [5]. The bottom graph in Fig. 6 shows the cross correlation of the two. There is a strong correlation between $C(t)$ and $\Delta T(t)$; the maximum correlation is about 70% of the peak value of the autocorrelations. The interpretation is as follows: As the pattern became more organized relative to the ordered time-averaged pat-

tern, the heat transport of the system was enhanced. Since a constant amount of heat was being supplied, this resulted in a decrease of the bottom temperature and thus the temperature difference. The large fluctuations in $C(t)$ and $\Delta T(t)$ corresponded to KL transitions since the patterns were most disorganized during those transitions [12]. This result showed that order and fluctuations of the patterns, as defined relative to the time average, were physically meaningful quantities of the spatiotemporally chaotic system.

We wish to thank N. B. Tuffiaro for bringing our attention to time averaging of chaotic patterns, and to J. Gollub for sharing the results of his group with us before publication. This work was funded by the U.S. Department of Energy and a UC/INCOR grant.

*Permanent address: Department of Physics, University of California, Santa Barbara, CA 93106.

- [1] M. C. Cross and P. C. Hohenberg, *Rev. Mod. Phys.* (to be published).
- [2] S. Ciliberto and P. Bigazzi, *Phys. Rev. Lett.* **60**, 286 (1988); M. Caponeri and S. Ciliberto, *Physica (Amsterdam)* **58D**, 365 (1992).
- [3] N. B. Tuffiaro, R. Ramshankar, and J. P. Gollub, *Phys. Rev. Lett.* **62**, 422 (1989).
- [4] M. Dubois, F. Daviaud, and M. Bonettie, *Phys. Rev. A* **42**, 3388 (1990).
- [5] B. J. Gluckman, P. Marcq, J. Bridger, and J. P. Gollub, *Phys. Rev. Lett.* **71**, 2034 (1993).
- [6] G. Küppers and D. Lortz, *J. Fluid Mech.* **35**, 609 (1969).
- [7] L. Ning and R. E. Ecke, *Phys. Rev. E* **47**, 3326 (1993).
- [8] F. Zhong, R. E. Ecke, and V. Steinberg, *J. Fluid Mech.* **249**, 135 (1993).
- [9] Y. Hu, R. E. Ecke, and G. Ahlers (to be published).
- [10] P. Chossat and M. Golubitsky, *Physica (Amsterdam)* **32D**, 423 (1988).
- [11] G. Ahlers, M. C. Cross, P. C. Hohenberg, and S. Safran, *J. Fluid Mech.* **110**, 297 (1981); M. C. Cross, P. C. Hohenberg, and M. C. Lücke, *J. Fluid Mech.* **136**, 169 (1983); V. Steinberg, G. Ahlers, and D. S. Cannell, *Phys. Scr.* **32**, 534 (1985).
- [12] F. Zhong and R. E. Ecke, *Chaos* **2**, 163 (1992).

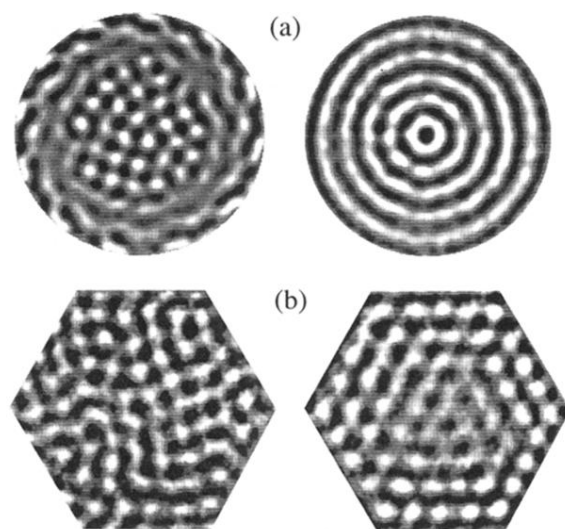
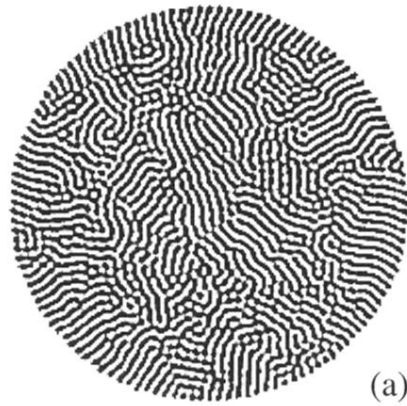
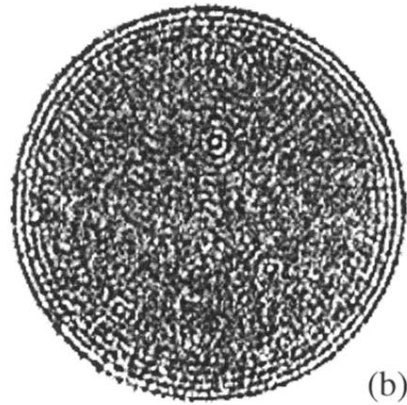


FIG. 1. The instantaneous (left) and time-averaged (right) patterns in rotating Rayleigh-Bénard convection in (a) the cylindrical container CW at $\Omega = 1090$ and $\epsilon = 0.053$ with water; (b) the hexagonal container HC at $\Omega = 150$ and $\epsilon = 0.08$ with carbon dioxide.



(a)



(b)

FIG. 2. The instantaneous (top) and time-averaged (bottom) patterns in rotating Rayleigh-Bénard convection in the cylindrical container CC ($\Gamma=41$) at $\Omega=16$ and $\epsilon=0.10$ with CO_2 . The time average is obtained from 720 images covering 6 h.

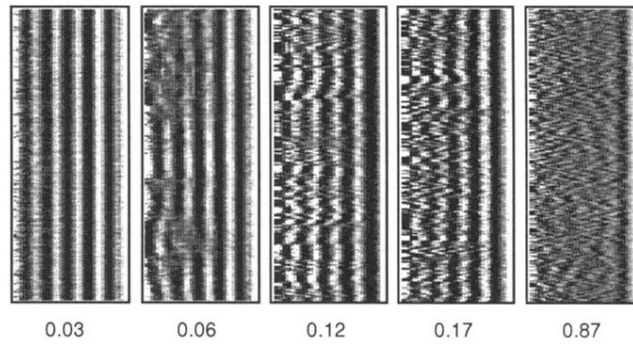


FIG. 4. Space-time plots of the azimuthally averaged intensities of the instantaneous patterns at a few labeled ϵ in the cylindrical container CC ($\Gamma=4.5$). In each plot, the center of the container is at the left edge and the wall is at the right edge, and time goes up. The time span is 3000 s. All the images are digitally enhanced.